



# A case study of hybrid manufacturing of a Ti-6Al-4V titanium alloy hip prosthesis

António José Festas<sup>1</sup> · Daniel Amaral Figueiredo<sup>1</sup> · Sílvia Ribeiro Carvalho<sup>1</sup> · Thang Hoang Vo<sup>2</sup> · Pierre-Thomas Dautre<sup>2</sup> · François Villeneuve<sup>2</sup> · António Manuel Ramos<sup>1,3</sup> · João Paulo Davim<sup>1</sup>

Received: 21 July 2023 / Accepted: 27 October 2023 / Published online: 9 November 2023  
© The Author(s) 2023

## Abstract

Hybrid manufacturing (HM) is a process that combines additive manufacturing (AM) and subtractive manufacturing (SM). It is becoming increasingly recognized as a solution capable of producing components of high geometric complexity, while at the same time ensuring the quality of the surface finish, rigour and geometric tolerance on functional surfaces. This work aims to study the surface finish quality of an orthopaedic hip resurfacing prosthesis obtained by HM. For this purpose, test samples of titanium alloy Ti-6Al-4V using two Power Bed Fusion (PBF) processes were manufactured, which were finished by turning and 5-axis milling. It was verified that, upon the machining tests, no differences in Ra and Rt were found between the various types of AM. Regarding the type of SM used, 5-axis milling provided lower roughness results with a consistent value of Ra=0.6 µm. The use of segmented circle mills in 5-axis milling proved to be an asset in achieving a good surface finish. This work successfully validated the concept of HM to produce a medical device, namely, an orthopaedic hip prosthesis. As far as surface quality is concerned, it could be concluded that the optimal solution for this case study is 5-axis milling.

**Keywords** Ti-6Al-4V · Titanium alloy · Hybrid manufacturing · EBM · SLS

## 1 Introduction

Hybrid manufacturing (HM) comprises the manufacture of a component or part in a sequence of production stages where the transition between additive manufacturing (AM) methods and subtractive manufacturing (SM) methods occurs [1]. The use of a sequence of the two manufacturing methods mentioned above allows the obtaining of parts or components of high geometric complexity, dimensional precision and surface finish [1, 2].

The use of 3D printing, also known as AM, has resulted in increased prominence and importance for the application of HM methods in creating medical devices [3, 4]. The use of AM, in which the part is manufactured by fusing the

material in layers, allows obtaining more intricate geometry components otherwise impossible to be achieved by SM. The production of components, such as orthopaedic implants, customized for each patient will enhance its integration, leading to a significant decrease in manufacturing time and material usage [5, 6].

Several AM processes are currently available, including electron beam melting (EBM) and selective laser sintering (SLS), both of which fit into the powder bed type of fusion (PBF) processes. The production process in this type of manufacturing involves using either a laser or electron beam to melt the powder, layer by layer to, in order to produce the component [7]. Among the AM processes, those of PBF are widely regarded as the most suitable for implant fabrication, as they allow the manufacture of components with porosity, which is a crucial factor for osseointegration and consequent success of the surgical intervention [8].

To prevent corrosion of the manufactured parts, EBM is carried out in a vacuum chamber which limits the size of the parts. Due to a larger beam, EBM allows for higher productivity but with poor surface finish. On the other hand, SLS, the beam, can be adjusted to the required speed or accuracy; however, the high internal stresses in the fabricated parts

✉ António José Festas  
afestas@ua.pt

<sup>1</sup> Department of Mechanical Engineering, Campus Santiago, University of Aveiro, 3810-193 Aveiro, Portugal

<sup>2</sup> University of Grenoble Alpes, CNRS, Grenoble INP, G-SCOP, 38000 Grenoble, France

<sup>3</sup> Biomechanics Research Lab, TEMA, University of Aveiro, Aveiro, Portugal

require post-treatment such as annealing to relieve these residual stresses. Comparing the two processes, the parts obtained by EBM have greater hardness and less porosity [9, 10].

Despite the benefits afforded to manufacturing by AM, certain limitations remain regarding repeatability, high dimensional accuracy, good surface finish and high productivity [11–13]. To fulfil functional requirements, a complementary manufacturing method, such as SM, may be necessary to obtain a part with all the requirements for its use.

In SM methods, excess material is removed by milling, turning or drilling operations. The use of CNC allows to achieve high levels of dimensional accuracy or tolerance and to improve surface quality [14–17]. However, this process is limited by the inability to achieve highly complex geometries, an economic factor related to material waste and work preparation. In the case of machining designated hard-cutting materials such as titanium alloys, the machining time and the cost of tools are increased due to the premature wear caused by this type of material [18, 19].

Although a few reviews about hybrid manufacturing can be found such as Jayawardane et al. [20] about sustainability perspectives, Popov et al. [21] about HM of steels and alloys and Lauwers et al. [22] on hybrid processes in manufacturing and the accessibility of AM equipment is increasing, it is not common in the literature to find case studies of hybrid manufacturing such as that of Loyda et al., [17] where an experimental study on the manufacturing of an aerospace component was conducted, specifically a titanium load-bearing bracket through hybrid manufacturing. A laser power bed fusion (LPBF) was used followed by 5-axis milling. Findings indicated that the combination of these two manufacturing processes allowed for the creation of a lightweight component with complex geometry and met the requirements for surface quality and dimensional tolerance in the functional areas. Ahmad et al. [23] studied the role of porosity in the machinability of AM and compared it with wrought Ti-6Al-4V and concluded that a higher porosity level is negatively influential in tool life and surface roughness. Lizzul et al. [24] studied the anisotropy effect on the surface quality of milled AM Ti-6Al-4V test samples and concluded that better machinability is attained for horizontal orientation. Dabwan et al. [25] studied the effect of layer orientation on turning a complex profile produced by EBM and found that surface finish and integrity are improved, but chip thickness is higher and flank wear has a higher degree for components manufactured along across-layer orientation.

Therefore, and in the context of HM, this study aimed to manufacture a resurfacing-type prosthesis. For the initial phase, EBM and SLS were used to produce the primary shape, which was then machined by turning and 5-axis milling to machine the surface that is in contact with the

acetabular component. Surface quality was considered the indicator of the work performed and the quality obtained.

The novelty of the presented work is the application of HM methods in the production of a frequently used medical device, namely a titanium alloy hip prosthesis. This is achieved through the combination of two AM processes and two SM processes, with an emphasis on 5-axis machining and the use of segmented circle mills. The study, while providing information that is still limited in the literature in this field, enabled to enhance the understanding of HM with tangible findings, which could support not only forthcoming research in this particular domain but also have potential for industrial implementation.

## 2 Experimental methodology

The work here presented is a case study based on an experimental approach to machining issues in titanium alloy components obtained through two distinct AM processes. The combination of these characteristics constitutes the added value and originality of this work in the field of scientific research.

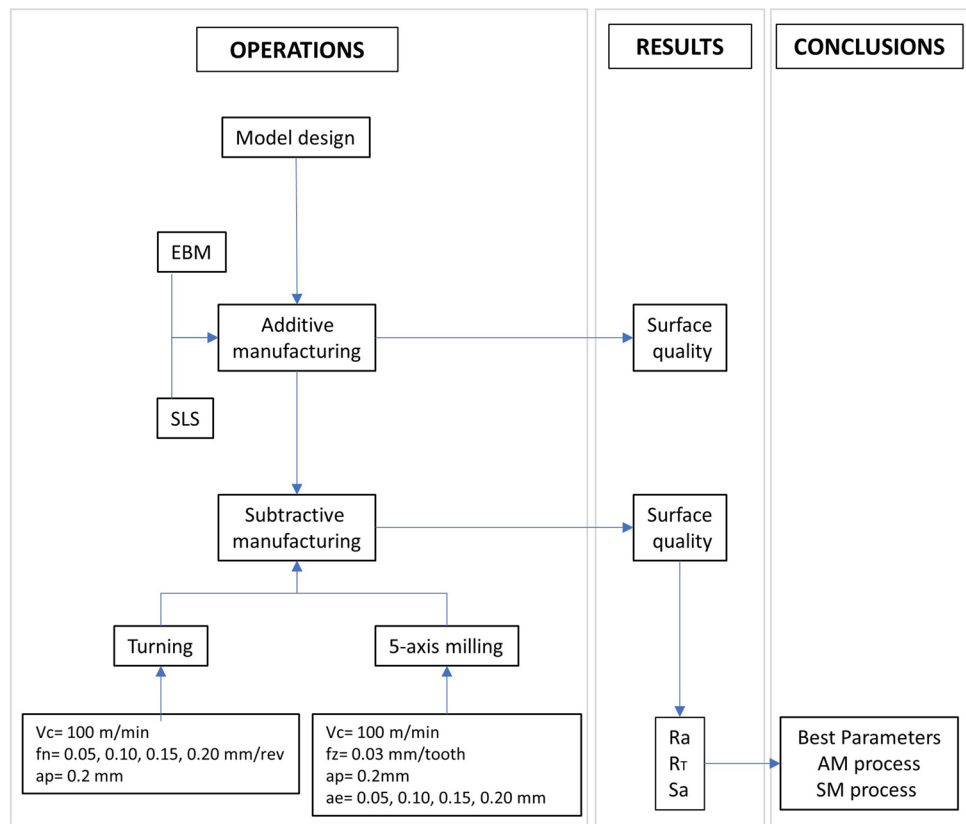
### 2.1 Methodology

The sequence of works carried out is represented in Fig. 1. Starting with the design of the prosthesis model, followed by the production by EBM and SLS and then ensuing machining by turning and 5-axis milling, the cutting parameters were chosen as recommended by the cutting tool manufacturer. The surface quality was measured previously and after machining tests with the use of an optical profiler. The strategy that best suits the intended objective was chosen based on the analysis of the results obtained where the determining factor was the lowest roughness value.

### 2.2 Materials and test samples

The piece to be machined was based on a resurfacing-type prosthesis used in total hip arthroplasty. The model used for this work has no other purpose than to serve for machining tests and was based in commercial implants design. The standard dimension for the outer diameter was defined as of 57 mm. In AM production, 1 mm was added to the radius and then removed by SM. The design of the model for machining was based on the DUROM™ model that dates back to 1997 and has been used clinically since 2001 without any modifications to its geometry. This model was created by optimizing previous models that had a history of poor performance leading to implant loosening and femoral neck fractures [26].

Fig. 1 Experimental flowchart



The test samples, made of titanium alloy Ti-6Al-4V, used in this work were obtained by EBM and SLS. For the intended purpose, 4 samples of each process were produced. The SLS test samples were produced in a General Electric M1, and the EBM in an ARCAM A1. The parameters selected are those that ensure the best material health. They are recommended by the machine manufacturers for the TA6V and the geometry to be produce. Previous experiments evaluated the production quality of geometries with suspended elements in Ti-6Al-4V alloy using additive manufacturing [27]. The manufacturing parameters of both EBM and SLS processes are in Table 1.

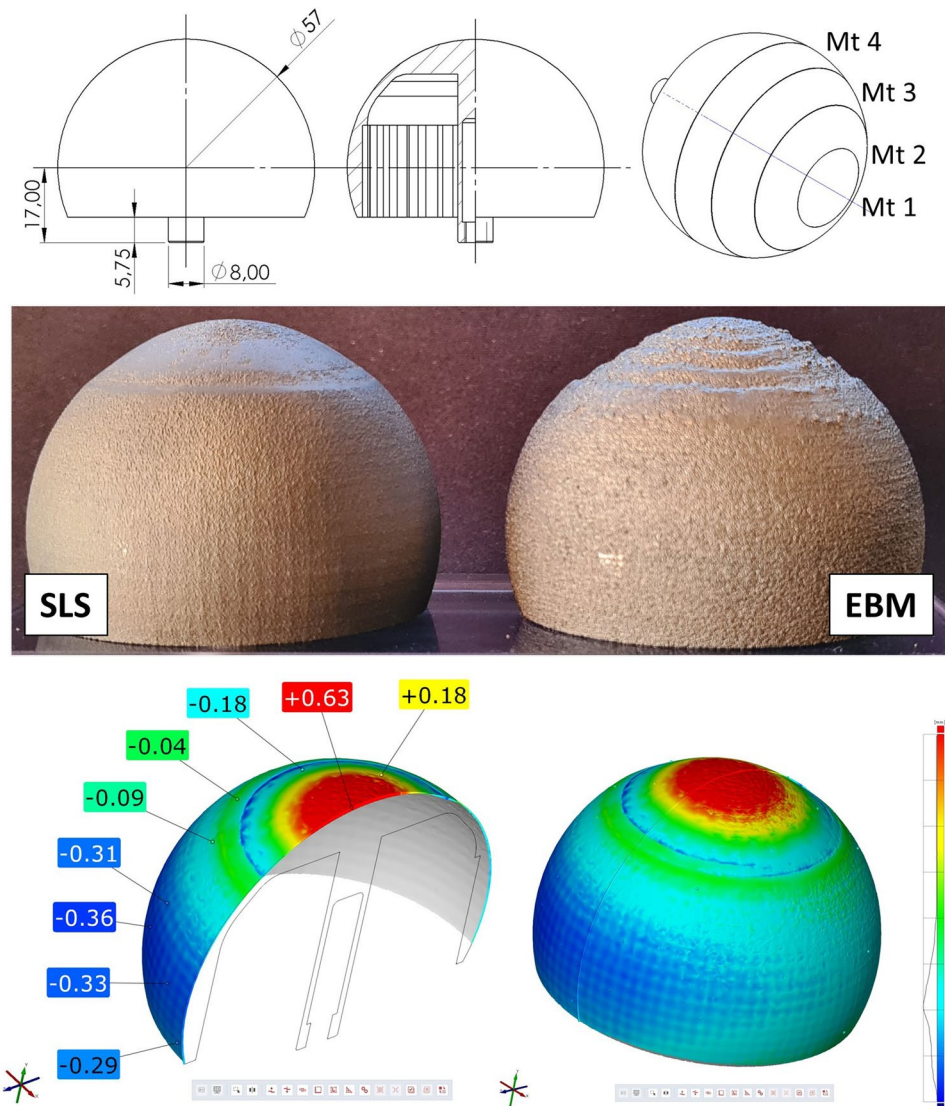
Figure 2 displays a simplified CAD drawing of the model including general dimensions, and a scheme of the machining tests (Mt) location on the test sample. There are also images of two test samples for each AM process, in which the surface texture differences and scaffold removal marks can be observed and an example of the geometric deviation of an SLS test sample compared to the CAD model. Manufacturing defects are visible, particularly at the end opposite the bone fixation rod. These defects are attributable to the printing process of the test samples, in which, due to the spherical outer geometry, it was necessary to build support scaffolding. The scaffolding was later removed, and it is apparent that the EBM test samples exhibit more pronounced marks as well as the deformation caused by these scaffolds

Table 1 AM parameters

Parameters	EBM	SLS
Layer thickness	50 µm	60 µm
Beam/laser power	Inner contour: 10mA; Outer contour: 4 mA	200 W
Beam/laser speed	Inner contour: 800 mm/s; Outer contour: 340 mm/s	1500 mm/s
Manufacturing substrate temperature	750 °C	170 °C
Powder granulometry	40–120 µm	D10 > 20 µm; D90 < 50 µm

than the SLS test samples. Additionally, the material used in SLS testing undergoes shrinkage during the cooling phase after melting [28]. The contraction will be higher where there is a higher concentration of fused material. This is particularly true in the region where scaffolds are utilized to support the part’s production, resulting in an increased amount of fused material. Consequently, the contraction in this area will be more substantial. In the case of components produced by EBM, the observed deformations are not of thermal origin but rather by the type of geometry that promotes the presence of unsupported surfaces despite the

**Fig. 2** Resurfacing prosthesis model, SLS and EBM test samples and an example of geometric deviations of an SLS test sample



introduction of scaffolds during the manufacturing process. Regarding the dimensions, while in the internal geometries, there was a very satisfactory accuracy with differences of approximately 0.1 mm compared to the CAD model sent for manufacture. However, the external surfaces exhibited a discrepancy of approximately 0.5 mm less concerning the desired additive manufacturing dimension. The comparative analysis of the CAD model was carried out using GOM's Atos Q 3D measuring equipment.

### 2.3 Machine tools, cutting tools and cutting parameters

#### 2.3.1 Machine tools

For the milling tests, a Haas UMC 500 5-axis machining center was used, with 22.4 kW of power, 10,000 rpm of maximum speed and a maximum cutting feedrate of 16.5

m/min. Similar to that performed in the turning tests, in the 5-axis milling tests, 4 machining regions were considered in each test piece.

For the turning test, a Kingsbury MHP50 turning center was used, with 18 kW of power and 4000 rpm of maximum speed. In this case, the finished surface was achieved after two passes of the cutting tool, one for pre-finishing and the other for finishing. The first pass created a standard surface by eliminating the major surface defects obtained by AM.

#### 2.3.2 Cutting tools

For milling tests, a circle segmented or lens mill was used, with a 10-mm cylindrical shank, a tip radius of 20 mm with a 1-mm corner radius and 3 cutting edges and AICrN 3  $\mu$ m PVD-HiPIMS coating (HXD30GLENS 3 100 10 R20 from Palbit([www.palbit.pt](http://www.palbit.pt))). The tool manufacturer recommends that the tool be oriented  $8^\circ$  off the main axis orthogonal to



the surface of the part to avoid cutting at the center of the tool where the cutting speed is 0. This condition is possible to be achieved through the CAM software. For the turning tests, a 55° rhombic carbide insert was used, with 0.8 mm of tool tip radius, a 15° back rake angle, negative GS chip breaker and TiAlSiN 3 μm PVD-HiPIMS coating (DNMG 110408-GS PHH910 from Palbit cutting tools).

Figure 3 presents the machine tools and cutting tools used in the machining tests.

### 2.3.3 Cutting parameters

While the cutting speed, feedrate and machining strategy were maintained the same; on the milling cutting test, a different radial depth of cut ( $a_e$ ) was considered. The values of  $a_e$  chosen for the milling tests were based on the feedrate values of the turning tests. When executing the CAM program using Powermill, a helical cutting strategy was defined to ensure identical tool displacement along the part during milling and turning. In this way, for each value of  $f_r$ , there

is a corresponding identical value of  $a_e$ . Therefore, even though two different machining processes were used, it was possible to have identical tool paths on the material surface, allowing comparison of the obtained roughness values obtained. Table 2 presents the machining test planning and cutting parameters.

Due to the surface defects observed in the test samples in both AM processes, with greater relevance in the EBM, it was necessary to perform a surface normalization of the specimens used in the milling tests with a cutting pass. This operation aimed to guarantee a constant depth of cut ( $a_p$ ) and  $a_e$  to be removed by the tool and thus avoid unexpected changes in this parameter which could potentially compromise tool integrity and to ensure surface evenness.

To calculate the spindle speed, the value of the cutting speed and the tool diameter are required. By default, for the control of the cutting speed, the effective diameter of the cut was considered and corresponding to the cutting diameter at cutting depth ( $a_p$ ). Figure 4 shows the positional relationship between the cutting tool and the test

**Fig. 3** a Kingsbury MHP50 turning center, b HAAS UMC 500 machining center, c turning insert DNMG 110408-GS PHH910 geometry, d mill cutter HXD30GLENS 3 100 10 R20 geometry.

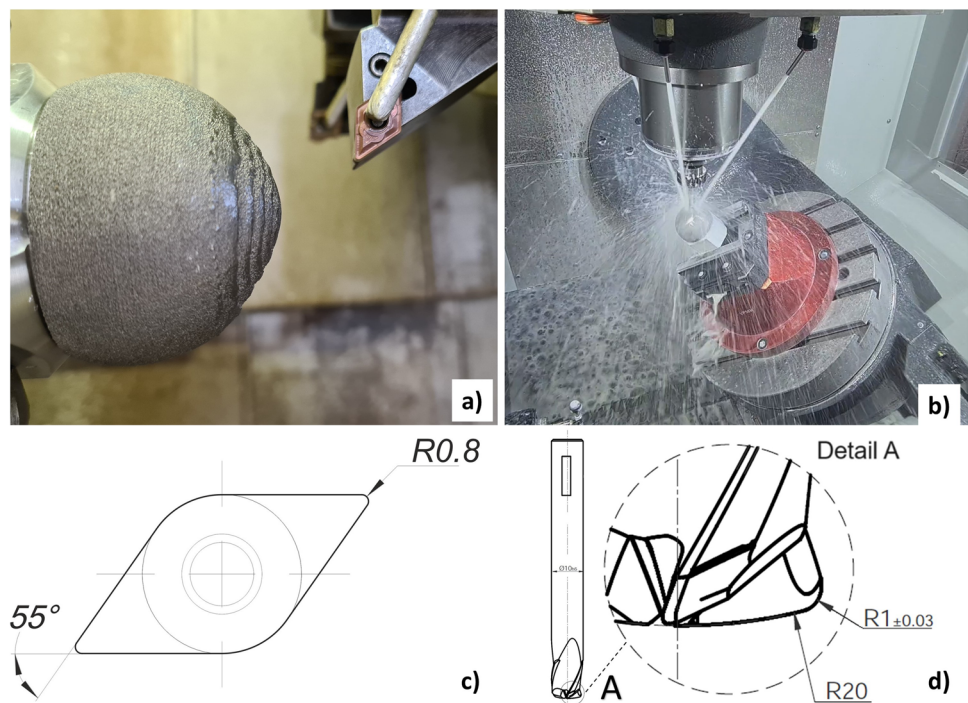


**Table 2** Machining test planning

	Turning			Milling			
	Vc (m/min)	$f_r$ (mm/rev)	$a_p$ (mm)	Vc (m/min)	$f_z$ (mm/tooth)	$a_p$ (mm)	$a_e$ (mm)
Mt 1	100	0.05	0.2	100	0.03	0.2	0.05
Mt 2	100	0.1	0.2	100	0.03	0.2	0.1
Mt 3	100	0.15	0.2	100	0.03	0.2	0.15
Mt 4	100	0.20	0.2	100	0.03	0.2	0.20

Mt machining test.

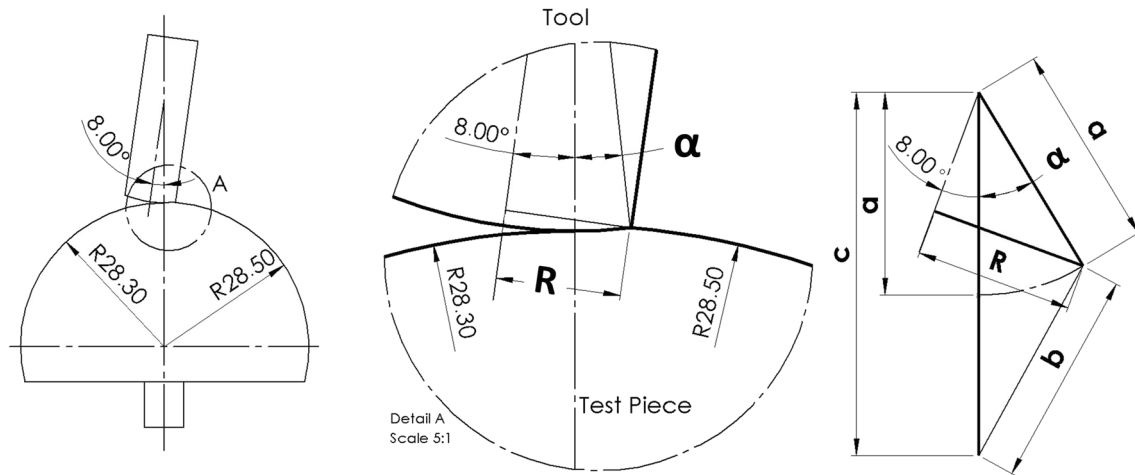


**Fig. 4** Cutting tool radius calculation

piece, as well as the dimensions of this relationship. The angle  $\alpha$  had to be determined using the cosine Eq. (1). By adding the  $8^\circ$  deviation imposed on the tool axis to this value, it was possible to establish Eq. (2) the maximum contact radius and thus the diameter of the contact.

$$a^2 = b^2 + c^2 - 2abc\cos\alpha \quad (1)$$

where  $a = 28.5$  mm,  $b = 20$  mm and  $c = 48.3$  mm. It was then possible to determine that  $\alpha = 6.28^\circ$ . Adding  $8^\circ$  from tool tilt angle, and considering 20 mm from tool radius, then  $R = 4.9$  mm then  $\varnothing = 9.8$  mm.

$$\sin(6.28 + 8) = \frac{R}{20} \quad (2)$$

For each milling test, a new tool was used, and for each turning section, a new cutting edge was applied. In total, 4 cutters and 4 turning inserts were used, where each insert has 4 cutting edges. For the execution of the machining tests, it was necessary to build an aluminium positioning and fixation device, to perform as a zero-point system, that allowed the test samples to be held always in the same position. The fixation of these to the device was performed through a screwed connection on the fixation rod. To machine the internal thread, it was necessary to make a hole, an operation that was done through helical milling [29]. The function of this device was to minimize positioning errors, or to ensure that the error was consistent across all the machining tests. Also, it was designed so that it could be used for both turning and 5-axis milling tests.

All milling and turning machining tests were conducted with the use of a water emulsion coolant containing emulsifying oil (RHENUS FU 51) at a concentration of 6%.

## 2.4 Surface roughness

Surface roughness measurements were taken before and after machining using an Alicona Infinity Focus SL optical 3D measurement system with  $10\times$  objective. For this work, three roughness parameters were analyzed: arithmetical mean height ( $R_a$ ), total height of profile ( $R_t$ ) and areal average roughness ( $S_a$ ). Due to the high surface roughness of the surfaces generated by the additive manufacturing processes, measuring the roughness using a contact roughness meter is not advisable as it may lead to damage the roughness meter's contact gauges. Thus, it is advisable to use the optical measuring equipment such as the one used in this phase of the work. Figure 5 presents the initial state of the surfaces prior to any machining operation. To quantify the roughness of the surfaces, several measurements were taken. For SLS,  $R_a = 4.61$   $\mu\text{m}$ ,  $R_t = 32.11$   $\mu\text{m}$  and  $S_a = 5.58$   $\mu\text{m}$ ; for EBM,  $R_a = 14.94$   $\mu\text{m}$ ,  $R_t = 84.78$   $\mu\text{m}$  and  $S_a = 18.82$   $\mu\text{m}$ .

## 2.5 Statistical analysis

As shown in Fig. 6, after the roughness measurements, the dataset was uploaded to statistical software R (v4.0.3) for further analysis. Paired hypothesis testing was employed to understand if there was a noteworthy difference in the surface finish ( $R_a$ ,  $R_t$ ,  $S_a$ ) of EBM and SLS samples obtained through turning and milling operations. The samples were paired in four ways, (1) milling samples of EBM and SLS, (2) turning samples of EBM and SLS, (3) EBM samples processed by turning and milling and (4) SLS samples that underwent turning and milling. In addition, the following null hypotheses were considered: "Is there no significant difference in the roughness of (1) milled surfaces attained



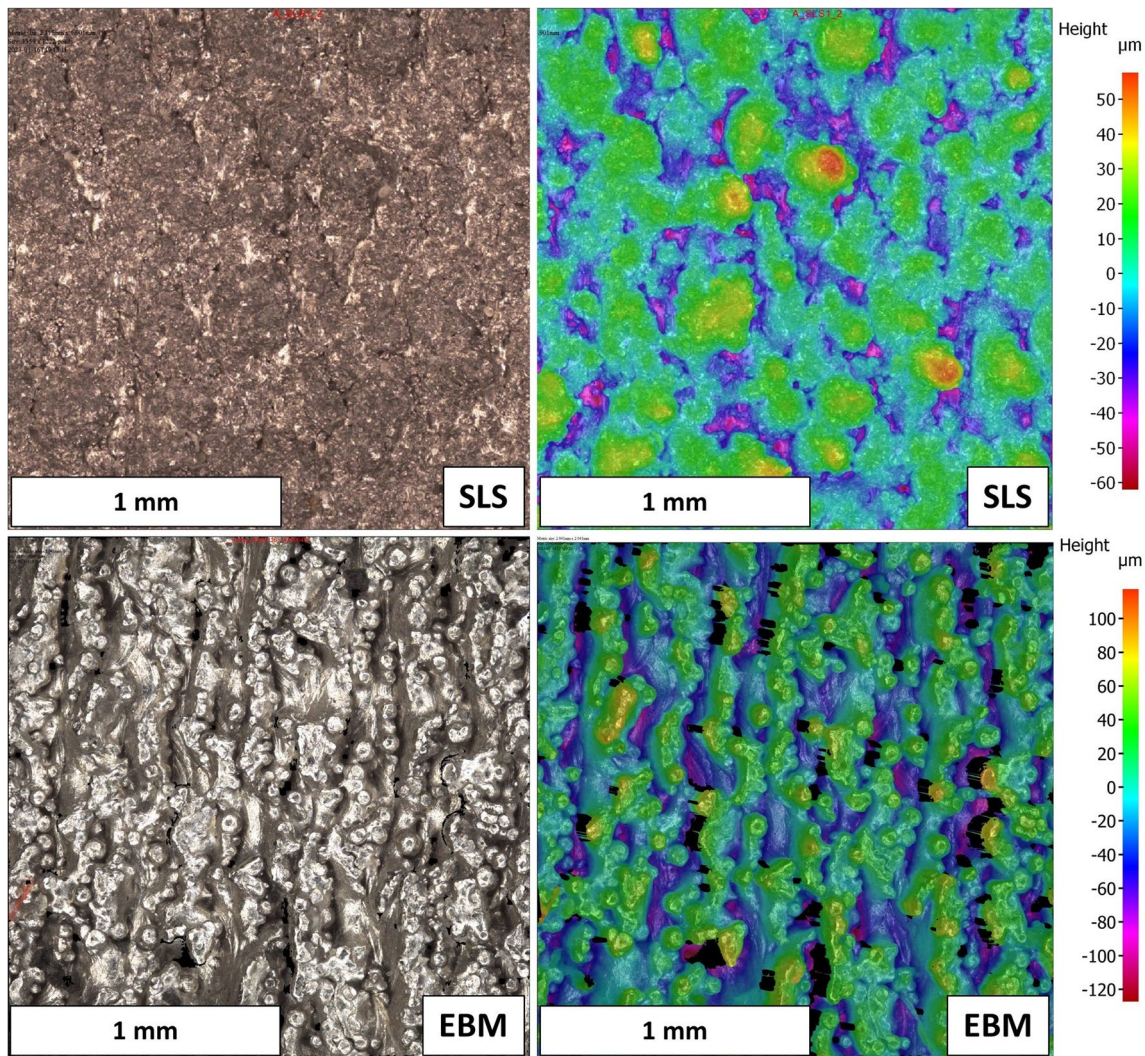
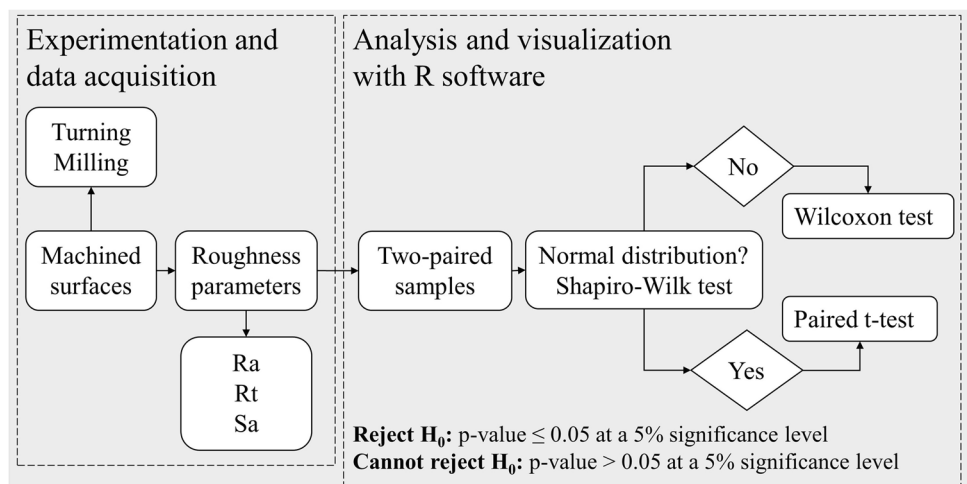


Fig. 5 SLS and EBM pre-machining surfaces

Fig. 6 Methodology for roughness data treatment and analysis



with EBM and SLS? (2) turned surfaces attained with EBM and SLS? (3) EBM samples attained with turning and milling? (4) SLS samples attained with turning and milling?”.

As presented in Fig. 6, the null hypothesis ( $H_0$ ) was rejected in favour of the alternative hypothesis ( $H_1$ ) when the  $p$ -value from the relevant test statistic, be it paired  $t$  test, or Wilcoxon test was either less than or equal to the defined significance level. Otherwise, when the  $p$ -value  $> 0.05$ , the null hypothesis was not rejected. Figure 5 also shows that, when the paired differences followed a normal distribution, the paired  $t$  test was applied; otherwise, the non-parametric Wilcoxon signed-rank test was used to assess if the paired groups were different from one another in a statistically significant manner. The normality of the paired samples was examined using the Shapiro–Wilk test.

### 3 Results and discussion

In Fig. 7, it is possible to observe the evolution of the roughness values  $R_a$  and  $R_t$  and  $S_a$  obtained through the turning ( $T$ ) and milling ( $M$ ) machining tests.

By examining the images presented, it is possible to make several different observations. The measured roughness values consistently surpass those found in milling during turning. This stands for the three roughness parameters employed for comparison.

Additionally, it is evident that turning the influence of the variant cutting parameter is more pronounced than in the case of milling. As can be seen, roughness in turning increases with the increase in feedrate. In the case of milling, roughness values remain almost constant even with an increase in feedrate.

The effects and importance of the impact of tool geometry parameters, namely tool nose radius variation on the surface finish of a machined part, have been widely researched, highlighting its significance and effects [30]. In the case presented here, where two tools with different geometries have been used with a distinguishable element as evident as the nose radius, it is appropriate to establish a correlation between this factor and the outcomes obtained. Consequently, in accordance with previous literature, it can be surmised that [31] it can be confirmed that the tool nose radius dimension has an inversely proportional influence on the roughness of a machined part surface.

It is notable that for the same type of subtractive manufacturing process, the type of additive manufacturing process does not have a significant impact on the measured roughness results.

Figure 8 displays diverse images of the machined surfaces for both additive manufacturing and of subtractive manufacturing types. The presented images, obtained through Alicona Infinity, relate to the tests conducted with  $a_c = 0.1$

mm for milling ( $M$ ) and  $f_r = 0.1$  mm/rev for turning ( $T$ ). In the case of turning, both for EBM and SLS, the displacement of the tool over the surface results in a distinct patterned texture with continuous and evenly spaced lanes from the cutting tool. In the case of milling, different effects can be observed for each additive manufacturing process. In the case of EBM, it is verifiable, similarly to turning, with some regularity in the marks left by the tool, however with shorter segments compared to turning. In the case of SLS, the formation of facets without any regular distribution is observable.

Figure 9 shows a side-by-side comparison of the surface images taken before machining, labelled “raw”, with those taken after milling ( $M$ ) and turning ( $T$ ) tests.

Regarding machining times, those observed in the turning tests exhibited significant superiority compared to those of 5-axis milling. Consequently, during turning, the following times were registered based on the conducted test:  $Mt1 \approx 5$  s,  $Mt2 \approx 7$  s,  $Mt3 \approx 7$  s,  $Mt4 \approx 7$  s. Correspondingly, in milling, the following times were recorded:  $Mt1 \approx 8$  min,  $Mt2 \approx 19$  min,  $Mt3 \approx 28$  min and  $Mt4 \approx 27$  min. It is evident that for this particular geometry, turning has a much higher productivity rate than milling.

#### 3.1 Data analysis

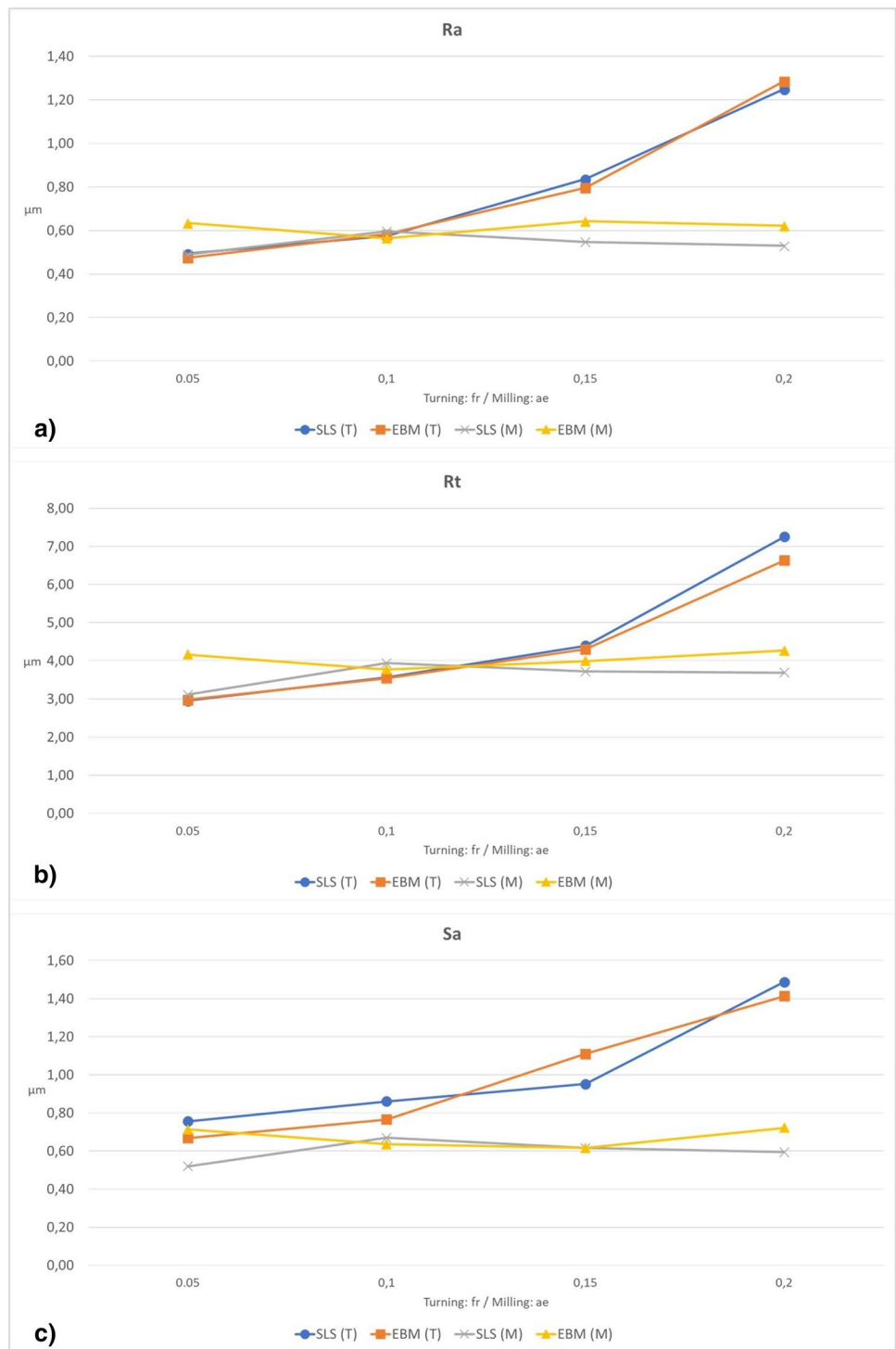
Figure 10 shows a boxplot visualization with the distribution for the surface roughness of printed samples (SLS and EBM) machined with milling and turning operations. Yellow squares ( $f_r$ , 0.05 mm/rev;  $a_c$ , 0.05 mm), blue circles ( $f_r$ , 0.10 mm/rev;  $a_c$ , 0.1 mm), red triangles ( $f_r$ , 0.15 mm/rev;  $a_c$ , 0.15 mm) and green crosses ( $f_r$ , 0.2 mm/rev;  $a_c$ , 0.2 mm) represent measurements from surfaces machined under the same feed rate (turning) and radial depth-of-cut (milling), each with a distinct colour and symbol.

Figure 10a–c indicates that roughness measurements for surfaces achieved by turning are grouped by colour, corresponding to the feed rate. Conversely, the distribution of the milling samples does not present the same tendency, as shown in Fig. 10d–f. It is well known that the surface roughness in turning depends on the feed rate ( $f_r$ ), which had four levels (0.05, 0.1, 0.15 and 0.2 mm/rev) in this work, while in milling, it varies on the feed per tooth ( $f_z$ ), which was constant during the process (0.03 mm/rev). On the other hand, the higher corner radius (20 mm) from the milling tools comparatively to the turning inserts (0.8 mm) contributed to reducing the roughness of the milling samples, as shown in Fig. 10g–i and j–l. In fact, for EBM samples, for example, one can see that the average arithmetical mean height ( $S_a$ ) for the milling samples was  $0.7 \pm 0.1 \mu\text{m}$ , while for the turning samples, it was  $1.1 \pm 0.3 \mu\text{m}$ .

The turning data from Fig. 10 presents a lower variability in  $S_a$  distribution per cluster compared to the arithmetical



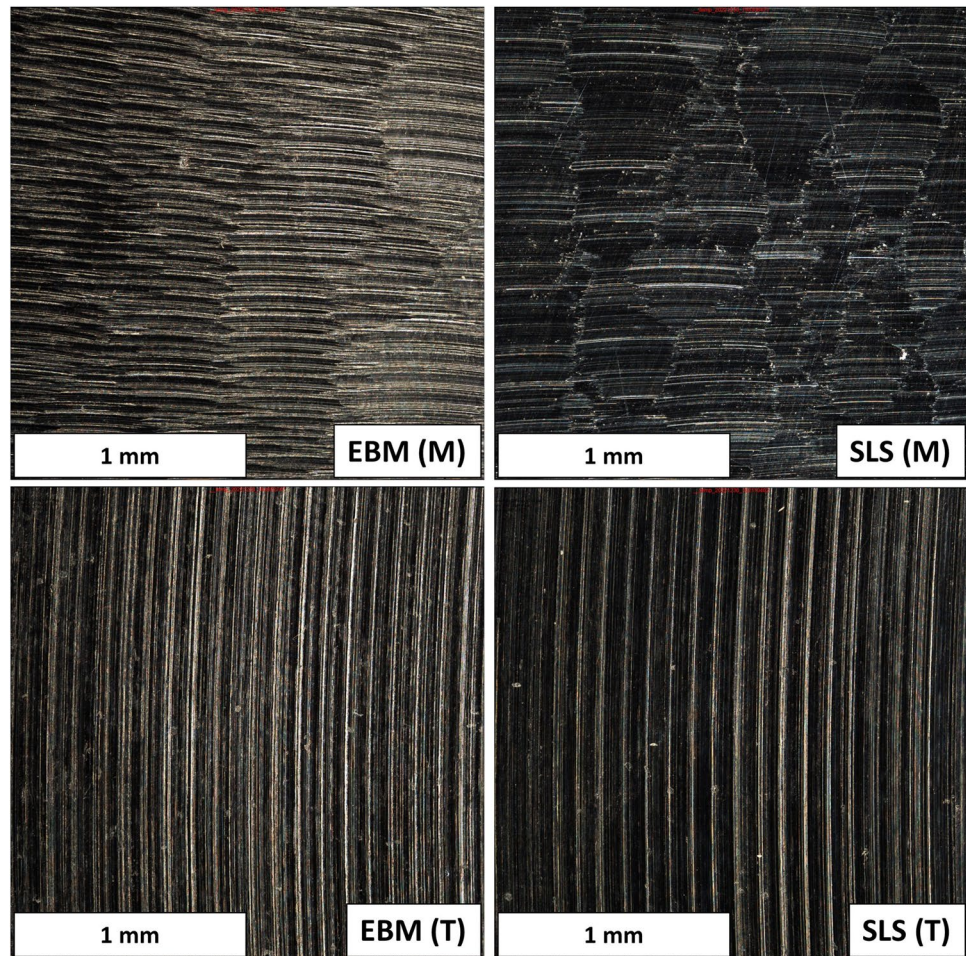
**Fig. 7** Roughness results **a** Ra, **b** Rt and **c** Sa for EBM and SLS test samples in turning (*T*) and milling (*M*)



mean height of a line (Ra), the Sa. For example, in the case of the SLS samples (Fig. 10a and c), the difference between the maximum and minimum Ra measurements was 0.17, 0.11, 0.14 and 0.32 μm for a feed rate of 0.05, 0.1, 0.15 and 0.2 mm/rev, respectively, while for Sa, it was 0.10, 0.10, 0.09 and 0.12 μm. This outcome was expected since the arithmetical mean height of an area (Sa) provides a greater

amount of information from the surface than the arithmetical mean height of a line (Ra). As a result, it is less prone to be affected outliers, such as surface defects. Another relevant remark regards the Rt parameter distribution for the turning and SLS samples, Fig. 10b and c, respectively, in which some outliers were observed. Since Rt is a geometrical parameter that evaluates the maximum peak-to-valley

**Fig. 8** Topographic analysis of machined surfaces by turning (*T*) and milling (*M*)



height over the evaluation length, it is more prone to detecting surface defects than the other parameters (*Sa*, *Ra*), which accounts for the presence of these outliers.

As mentioned before, the statistical inference was applied to assess how the combination between AM processes (SLS and EBM) and SM methods (turning or milling) would affect or not the surface roughness (*Ra*, *Rt*, *Sa*) of the part. It is worth mentioning that, when the paired differences followed a normal distribution, the parametric paired *t* test was used to compare the means; otherwise, the non-parametric Wilcoxon test was applied to compare the medians.

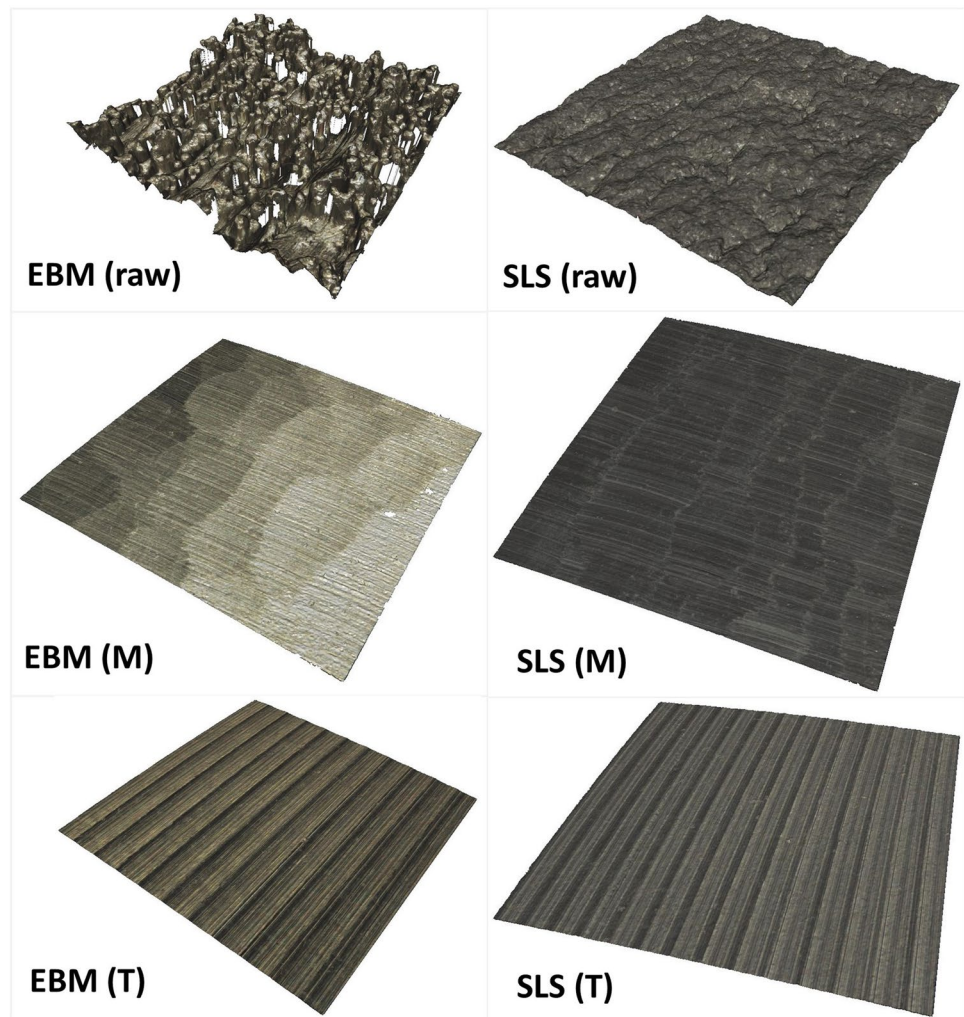
When evaluating whether altering the turning material, particularly when EBM or SLS samples would affect the achieved surface roughness, it was found that this would rely on the roughness parameter in analysis. Thereby, for *Ra* ( $p = 0.47$ ) and *Rt* ( $p = 0.52$ ), the median differences (Wilcoxon test) were not statistically significant. Nevertheless, for *Sa* ( $p = 0.04$ ), the mean differences (paired *t* test) proved to be statistically significant. That as expected, the obtained outcomes agree with the distributions from Fig. 10a–c. Lastly, these findings emphasize the importance

of combining linear (*Ra*, *Rt*) and spatial (*Sa*) roughness parameters for the evaluation of surface finish in biomedical components.

Regarding the samples processed by milling, it was found that altering the material that is EBM or SLS samples led to noteworthy variations in the mean surface roughness. The *p*-values attained in the paired *t* test were 0.01 for *Ra* and *Rt* and 0.002 for *Sa*. Actually, by observing the distribution from Fig. 10d–f, it is possible to see that the SLS samples presented much lower mean and median values than the EBM samples. Finally, under the tested conditions, the milling process exhibited greater responsiveness to material changes, resulting in a higher surface roughness than turning.

Similarly, the surface finish response of the EBM samples was found to depend on the roughness parameter when changing the processing strategy, i.e. turning or milling. Thereby, for *Ra* ( $p = 0.06$ ) and *Rt* ( $p = 0.34$ ), the differences (median and mean, respectively) were not statistically significant; however, for *Sa* ( $p = 0.0001$ ), it was statistically significant. It should be noted that as expected, these results

**Fig. 9** 3D microscopic analysis of the raw and machined surfaces by turning (*T*) and milling (*M*)



agree with the distributions from Fig. 10g–i. Additionally, this finding emphasizes the Sa responsiveness relative to the linear parameters. Lastly, the Sa distribution from Fig. 10i shows that turning produced greater surface roughness in EBM samples compared to milling.

In the case of the SLS samples, it was observed that for Ra ( $p = 0.0043$ ) and Sa ( $p = 0.00002$ ), the median differences were statically significant when changing the processing strategy, that is, turning or milling, while for Rt ( $p = 0.0789$ ), it did not present a significant difference. Similarly, to the observations made from the EBM samples, the turning process led to rougher surfaces for SLS samples, as illustrated in the Ra and Sa distribution from Fig. 10j and l. Finally, the results demonstrate that, under the tested conditions, the EBM and SLS samples responded similarly to the processing changes involving turning and milling regarding surface roughness. More

precisely, the respective statistical significances of the Sa and Rt differences varied altering the process for both material samples.

## 4 Conclusions

This work aimed to conduct a comparative experimental study of the manufacture of a resurfacing type prosthesis in titanium alloy Ti-6Al-4V using hybrid manufacturing. For this purpose, test samples produced through EBM and SLS were used, subsequently subjected to machining by turning and 5-axis milling. The potential for producing highly complex geometric parts using AM validates its use as a manufacturing process. Nevertheless, the extreme heterogeneity in terms of surface finish, mainly caused by the process itself, restricts its use in applications requiring



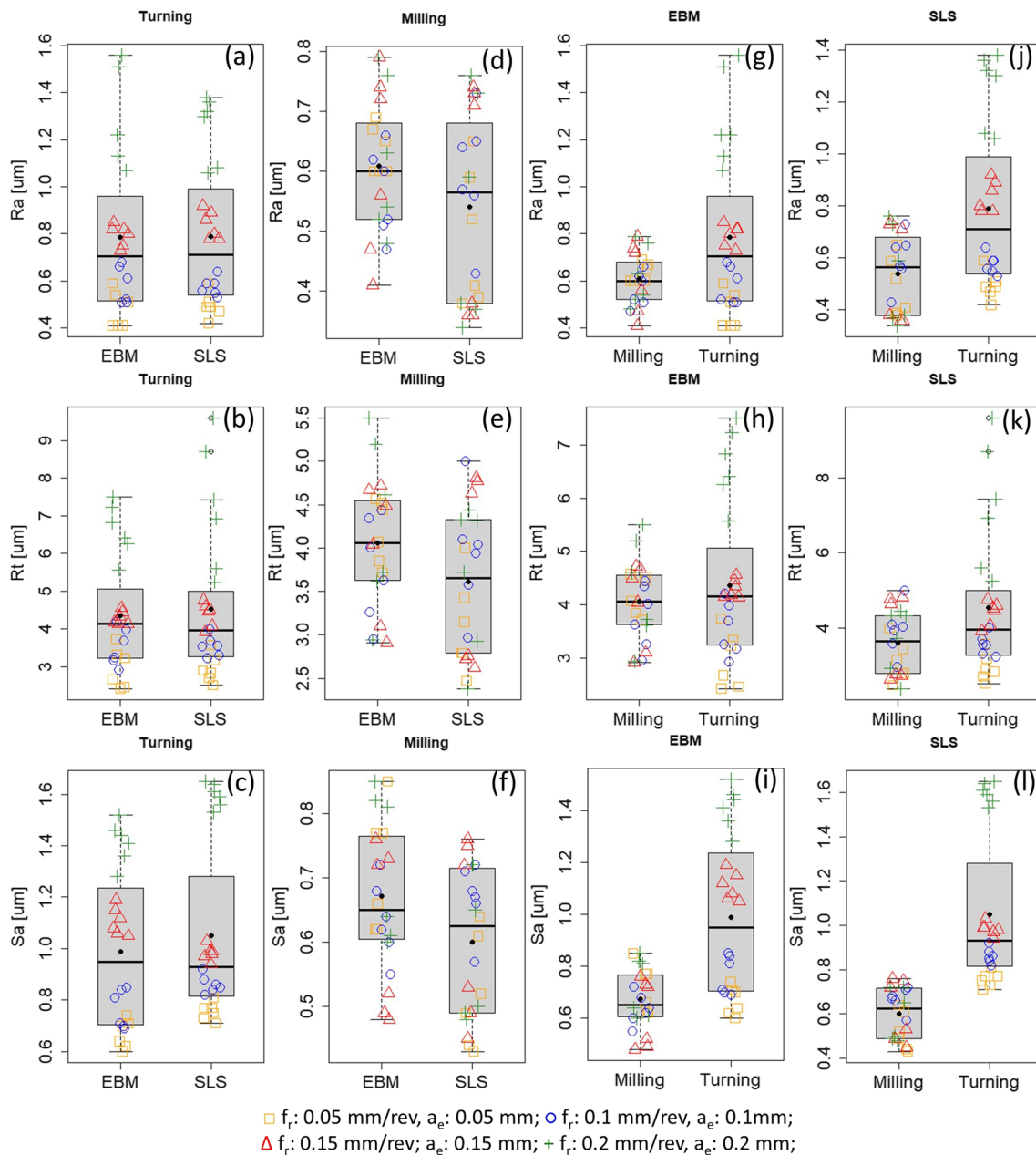


**Fig. 10** Roughness distribution (Ra, Rt and Sa) of turning samples (a–c), milling samples (d–f), EBM samples (g–i) and SLS samples (j–l)

high accuracy dimensional and geometric. To address this limitation and meet the mentioned requirements, it is essential to use SM processes that must be suitable for the final geometry of the part to be produced.

Regarding surface finish, irrespective of the SM process used, it was found that, if the roughness evaluation parameters Ra and Rt are taken into account, there were no discernible differences between components produced either by SLS or by EBM. However, according to the Sa parameter, the SLS test samples had better roughness results. Therefore, considering this evaluation parameter, the

choice of AM process must be made taking into account the advantages and disadvantages of each process and its suitability in ensuring the required quality of the finished product.

Concerning the SM process, it was verified that turning the roughness is directly dependent on the feedrate ( $f_r$ ), while in milling, the  $a_e$  has a minor influence on roughness; this findings are coherent to other results found in literature [32]. Also, this is related to the fact that in this work, segmented circle cutters were used, also referred to as lens cutters, in 5-axis milling. The results demonstrate

that this option provides several advantages compared to traditional ball cutters, based on the achieved surface finish [33]. The primary reason for the discrepancy in roughness outcomes between turning and milling was due to the use of a segmented circle milling cutter which has a much larger nose radius compared to the turning insert. In a direct comparison, the use of a larger radius on the cutting edge of the milling tool has a direct influence on the chip thickness of the material removed, thereby leading to a reduction in heat generation. This particular factor can prove beneficial in enhancing the machinability of Ti alloys and the capabilities of the processes.

When it comes to production time, turning results in a faster production rate, while 5-axis milling enables the creation of components with superior surface finish and complex geometries. This is particularly favourable for customized orthopaedic components.

**Acknowledgements** The authors acknowledge “Project No. 031556-FCT/SAICT/2017”; FAMASI – Sustainable and intelligent manufacturing by machining financed by the Foundation for Science and Technology (FCT), POCI, Portugal, in the scope of TEMA, Centre for Mechanical Technology and Automation – UID/EMS/00481/2013.

The authors would also like to thank Palbit for all the support given, both supplying the cutting tools and the availability to use their equipment. They would also like to acknowledge the support given by the companies S3D in digitizing the test samples and DimLaser in providing the SLS test samples

**Author contribution** AF: experimental work, conceptualization, methodology, writing—original draft preparation; DF: experimental work; SC: experimental work, writing; TV: experimental work; P-TD: experimental work; FV: experimental work; AR: conceptualization, supervision; J.PD: conceptualization, supervision.

**Funding** Open access funding provided by FCTIFCCN (b-on). This research was not supported by any funding.

**Data availability** Not applicable.

**Code availability** Not applicable.

## Declarations

**Competing interests** The authors declare no competing interests.

**Open Access** This article is licensed under a Creative Commons Attribution 4.0 International License, which permits use, sharing, adaptation, distribution and reproduction in any medium or format, as long as you give appropriate credit to the original author(s) and the source, provide a link to the Creative Commons licence, and indicate if changes were made. The images or other third party material in this article are included in the article’s Creative Commons licence, unless indicated otherwise in a credit line to the material. If material is not included in the article’s Creative Commons licence and your intended use is not permitted by statutory regulation or exceeds the permitted use, you will need to obtain permission directly from the copyright holder. To view a copy of this licence, visit <http://creativecommons.org/licenses/by/4.0/>.

## References

- Butt J, Shirvani H (2018) Additive, subtractive, and hybrid manufacturing processes. *Adv Manuf Process Mater Struct* 18:187–218. <https://doi.org/10.1201/b22020-9>
- Häfele T, Schneberger JH, Kaspar J, Vielhaber M, Griebisch J (2019) Hybrid additive manufacturing – process chain correlations and impacts. *Procedia CIRP* 84:328–334. <https://doi.org/10.1016/j.procir.2019.04.220>
- Bozkurt Y, Karayel E (2021) 3D printing technology; methods, biomedical applications, future opportunities and trends. *J Mater Res Technol* 14:1430–1450. <https://doi.org/10.1016/j.jmrt.2021.07.050>
- da Silva LRR, Sales WF, dos Anjos Rodrigues Campos F, de Sousa JAG, Davis R, Singh A et al (2021) A comprehensive review on additive manufacturing of medical devices. *Prog Addit Manuf* 6:517–53. <https://doi.org/10.1007/s40964-021-00188-0>
- Culmone C, Smit G, Breedveld P (2019) Additive manufacturing of medical instruments: a state-of-the-art review. *Addit Manuf* 27:461–473. <https://doi.org/10.1016/j.addma.2019.03.015>
- Lowther M, Louth S, Davey A, Hussain A, Ginestra P, Carter L et al (2019) Clinical, industrial, and research perspectives on powder bed fusion additively manufactured metal implants. *Addit Manuf* 28:565–584. <https://doi.org/10.1016/j.addma.2019.05.033>
- Dev Singh D, Mahender T, Raji RA (2021) Powder bed fusion process: a brief review. *Mater Today Proc* 46:350–355. <https://doi.org/10.1016/j.matpr.2020.08.415>
- Yilmaz B, Al Rashid A, Mou YA, Evis Z, Koç M (2021) Bioprinting: a review of processes, materials and applications. *Bioprinting* 23:e00148. <https://doi.org/10.1016/j.bprint.2021.e00148>
- Chen L-Y, Liang S-X, Liu Y, Zhang L-C (2021) Additive manufacturing of metallic lattice structures: unconstrained design, accurate fabrication, fascinated performances, and challenges. *Mater Sci Eng R Reports* 146:100648. <https://doi.org/10.1016/j.mser.2021.100648>
- Roudnicka M, Misurak M, Vojtech D (2019) Differences in the response of additively manufactured titanium alloy to heat treatment-comparison between SLM and EBM. *Manuf Technol* 19:668–73. <https://doi.org/10.21062/ujep/353.2019/a/1213-2489/MT/19/4/668>
- Dilberoglu UM, Haseltalab V, Yaman U, Dolen M (2019) Simulator of an additive and subtractive type of hybrid manufacturing system. *Procedia Manuf* 38:792–799. <https://doi.org/10.1016/j.promfg.2020.01.110>
- Essink WP, Flynn JM, Goguelin S, Dhokia V (2017) Hybrid ants: a new approach for geometry creation for additive and hybrid manufacturing. *Procedia CIRP* 60:199–204. <https://doi.org/10.1016/j.procir.2017.01.022>
- Lorenz KA, Jones JB, Wimpenny DI, Jackson MR (2015) A review of hybrid manufacturing. *Proc - 26th Annu Int Solid Free Fabr Symp - An Addit Manuf Conf SFF 2015* 2020:96–108.
- Joshi A, Anand S (2017) Geometric complexity based process selection for hybrid manufacturing. *Procedia Manuf* 10:578–589. <https://doi.org/10.1016/j.promfg.2017.07.056>
- Saptaji K, Gebremariam MA, Azhari MABM (2018) Machining of biocompatible materials: a review. *Int J Adv Manuf Technol* 97:2255–2292. <https://doi.org/10.1007/s00170-018-1973-2>
- Davis R, Singh A, Jackson MJ, Coelho RT, Prakash D, Charalambous CP, et al (2022) A comprehensive review on metallic implant biomaterials and their subtractive manufacturing. *Int J AdvManuf Technol* 120:1473–1530. <https://doi.org/10.1007/s00170-022-08770-8>

17. Loyda A, Arizmendi M, Ruiz de Galarreta S, Rodriguez-Florez N, Jimenez A (2023) Meeting high precision requirements of additively manufactured components through hybrid manufacturing. *CIRP J Manuf Sci Technol* 40:199–212. <https://doi.org/10.1016/j.cirpj.2022.11.011>
18. Pramanik A, Littlefair G (2015) Machining of titanium alloy (Ti-6Al-4V)-theory to application. *Mach Sci Technol* 19:1–49. <https://doi.org/10.1080/10910344.2014.991031>
19. Pramanik A (2014) Problems and solutions in machining of titanium alloys. *Int J Adv Manuf Technol* 70:919–928. <https://doi.org/10.1007/s00170-013-5326-x>
20. Jayawardane H, Davies IJ, Gamage JR, John M, Biswas WK (2023) Sustainability perspectives – a review of additive and subtractive manufacturing. *Sustain Manuf Serv Econ* 2:100015. <https://doi.org/10.1016/j.smse.2023.100015>
21. Popov VV, Fleisher A (2020) Hybrid additive manufacturing of steels and alloys. *Manuf Rev* 7:6. <https://doi.org/10.1051/mfrev/iew/2020005>
22. Lauwers B, Klocke F, Klink A, Tekkaya AE, Neugebauer R, McIntosh D (2014) Hybrid processes in manufacturing. *CIRP Ann - Manuf Technol* 63:561–583. <https://doi.org/10.1016/j.cirp.2014.05.003>
23. Ahmad S, Mujumdar S, Varghese V (2022) Role of porosity in machinability of additively manufactured Ti-6Al-4V. *Precis Eng* 76:397–406. <https://doi.org/10.1016/j.precisioneng.2022.04.010>
24. Lizzul L, Sorgato M, Bertolini R, Ghiotti A, Bruschi S (2021) Anisotropy effect of additively manufactured Ti6Al4V titanium alloy on surface quality after milling. *Precis Eng* 67:301–310. <https://doi.org/10.1016/j.precisioneng.2020.10.003>
25. Dabwan A, Anwar S, Al-Samhan AM, Alqahtani KN, Nasr MM, Kaid H, et al (2023) CNC turning of an additively manufactured complex profile Ti6Al4V component considering the effect of layer orientations. *Processes* 11(4):1031. <https://doi.org/10.3390/pr11041031>
26. Grigoris P, Roberts P, Panousis K (2006) The development of the Durom™ metal-on-metal hip resurfacing. *HIP Int* 16:65–72. <https://doi.org/10.1177/112070000601604s13>
27. Ledoux Y, Ghaoui S, Vo TH, Ballu A, Villeneuve F, Vignat F et al (2022) Geometrical defect analysis of overhang geometry produced by electron beam melting: experimental and statistical investigations. *Int J Adv Manuf Technol* 122:2059–2075. <https://doi.org/10.1007/s00170-022-10040-6>
28. Rupal BS, Anwer N, Secanell M, Qureshi AJ (2020) Geometric tolerance and manufacturing assemblability estimation of metal additive manufacturing (AM) processes. *Mater Des* 194:108842. <https://doi.org/10.1016/j.matdes.2020.108842>
29. Festas AJ, Pereira RB, Ramos A, Davim JP (2021) A study of the effect of conventional drilling and helical milling in surface quality in titanium Ti-6Al-4V and Ti-6Al-7Nb alloys for medical applications. *Arab J Sci Eng* 46:2361–2369. <https://doi.org/10.1007/s13369-020-05047-8>
30. Abdellaoui L, Khelifi H, Bouzid Sai W, Hamdi H (2020) Tool nose radius effects in turning process. *Mach Sci Technol* 25:1–30. <https://doi.org/10.1080/10910344.2020.1815038>
31. Mgherony A, Mikó B, Farkas G (2021) Comparison of surface roughness when turning and milling. *Period Polytech Mech Eng* 65:337–344. <https://doi.org/10.3311/PPME.17898>
32. Dikshit MK, Puri AB, Maity A (2017) Optimization of surface roughness in ball-end milling using teaching-learning-based optimization and response surface methodology. *Proc Inst Mech Eng Part B J Eng Manuf* 231:2596–2607. <https://doi.org/10.1177/0954405416634266>
33. Żurek P, Żurawski K, Szajna A, Flejszar R, Sałata M (2021) Comparison of surface topography after lens-shape end mill and ball endmill machining. *Technologia I Automatyizacja Montażu (Assembly Techniques and Technologies)* 114(4):9–15 <https://doi.org/10.15199/160.2021.4.2>

**Publisher's Note** Springer Nature remains neutral with regard to jurisdictional claims in published maps and institutional affiliations.